Comparing NKp44+ and NKp44− ILC3s in Human Lung Cancer via Transcriptional Sequencing

Hang Cheng
Jilin University First Hospital
Shan Zhu
Jilin University First Hospital
Chengyan Jin
Jilin University Second Hospital
Jing Wu
Jilin University First Hospital
Xinping Lv
Jilin University First Hospital
Tete Li
Jilin University First Hospital
Guoxia Zang
Jilin University First Hospital
Bao Gao
Jilin University First Hospital
Zhiguang Yang
Jilin University First Hospital
Jiuwei Cui
Jilin University First Hospital
Hideki Ueno
Icahn School of Medicine at Mount Sinai
Yong-Jun Liu
Jilin University First Hospital
Jingtao Chen (jtchen@jlu.edu.cn)
Jilin University https://orcid.org/0000-0002-4720-4225

Research Article

Keywords: Human lung cancer, NKp44+ ILC3s, NKp44− ILC3s, regional immunity, RNA sequence, tumor microenvironment.

Posted Date: October 8th, 2021

DOI: https://doi.org/10.21203/rs.3.rs-937649/v1

Comparing NKp44^{+} and NKp44^{-} ILC3s in human lung cancer via transcriptional sequencing

Hang Cheng[1, 2], Shan Zhu[1], Chengyan Jin[3], Jing Wu[1], Xinping Lv[1], Tete Li[1], Guoxia Zang[1], Bao Gao[1], Zhiguang Yang[4], Jiuwei Cui[5], Hideki Ueno[6], Yong-Jun Liu[1], Jingtao Chen[1,*]

[1] Institute of Translational Medicine, The First Hospital of Jilin University, Changchun 130061, China

[2] Department of Pediatrics, The First Hospital of Jilin University, Changchun 130021, China

[3] Department of Thoracic Surgery, The Second Hospital of Jilin University, Changchun 130041, China

[4] Department of Thoracic Surgery, The First Hospital of Jilin University, Changchun, 130021 China

[5] Cancer Center, The First Hospital, Jilin University, Changchun 130021, China

[6] Department of Microbiology, Icahn School of Medicine at Mount Sinai, New York, New York, USA

*** Corresponding and lead author:** jtchen@jlu.edu.cn

Acknowledgments

We are grateful to the patients for volunteering to participate in this study.

Abstract

Purpose Innate lymphoid cells (ILCs) play essential roles in mucosal innate immunity. The presence and function of ILCs in human lung cancer have not been extensively studied. This study aimed to identify and analyze the characteristics of the predominant subgroups in lung cancer .

Methods Single-cell suspensions were obtained from lung tissue diseased regions, non-diseased regions, and peripheral blood. The distribution of the ILC subgroups was analyzed by flow cytometry. The RNA of all samples was sequenced by BGI Group. Differentially expressed

genes (DEGs) were assessed by functional and pathway enrichment analyses.

Results ILC3s were exclusively increased in the lung cancer diseased region. The NKp44^{+} ILC3 subgroup was found in the diseased and non-diseased regions, but not in the peripheral blood. RNA sequencing indicated similar basic transcripts in NKp44^{-} ILC3s and NKp44^{+} ILC3s, but more enrichment in the signal transduction pathway and signaling molecules and interaction pathway in NKp44^{+} ILC3s. Compared with in NKp44^{-} ILC3s, gene transcripts tended to be upregulated in NKp44^{+} ILC3s in the Ras, RAP1, Jak-STAT, Notch, NF-κB, and Toll-like receptor signaling pathways and downregulated in the TGF-β signaling pathway. In the signaling molecules and interaction pathway, levels of most key molecules were higher in NKp44^{+} ILC3s in the cell adhesion molecules and cytokine-cytokine receptor interaction pathways.

Conclusion ILC3s was the dominant group in lung cancer and NKp44^{+}ILC3s was significant in diseased region. By transcripts analysis, the upregulated pathways in NKp44^{+} ILC3s enable survival, proliferation, activation, interleukin production, and antigen presentation. Our results provide the transcript landscape of DEGs in NKp44^{+} and NKp44^{-} ILC3s in lung cancer, providing a theoretical basis for further study of potential therapies.

Keywords: Human lung cancer, NKp44^{+} ILC3s, NKp44^{-} ILC3s, regional immunity, RNA sequence, tumor microenvironment.

Introduction

Lung cancer is an important disease in humans. The innate immune system of the lung mucosa is the front line of antitumor immunity. Innate lymphoid cells (ILCs) were recently discovered as new members of the mucosal innate immune system. ILCs are essential for mucosal surveillance, defense, and homeostasis (Eberl et al., 2015; Spits et al., 2013). Based on cytokine secretion ability and transcription factors that are essential for ILC development and maintenance, ILCs are classified into three groups. Group 1 ILCs (ILC1s) express the transcription factor T-bet and produce interferon-γ (IFN-γ) and TNF-α. Group 1 also can be said to include natural killer (NK) cells, which rely on the transcription factors T-bet and EOMES. Group 2 ILCs (ILC2s) secrete type 2 cytokines and are functionally regulated by GATA3. Group 3 ILCs (ILC3s) are characterized by RORγt, which produces IL-17, IL-22, or both (Spits et al., 2013; Spits and Cupedo, 2012).

ILCs play important roles in lung mucosal immunity and inflammation (Lai et al., 2016). Among the ILCs, NK cells have been the most widely studied. They are important contributors to host defense against tumors and viruses and are involved in asthma, chronic obstructive pulmonary disease, and bacterial resistance (Cong and Wei, 2019). ILC1s play a predominant role in the lung eliminating pathogens (Silver et al., 2016). ILC2s have the ability to maintain airway mucosal stability (Monticelli et al., 2011) and clear parasites (Maizels et al., 2012). ILC2s participate in the development of asthma (Scanlon and McKenzie, 2012) and pulmonary fibrosis (Hams et al., 2014; Wohlfahrt et al., 2016). ILC3s promote obesity and asthma by producing IL-17 (Kim et al., 2014), and they produce IL-17 and IL-22 to clear bacterial infections (Van Maele et al., 2014). In human lung cancer tissues, ILC3s produce IL-17, IL-22, and lymphotoxin, which have antitumor effects (Carrega et al., 2015).

However, the characteristics of human ILCs in the pulmonary tumor microenvironment have not been thoroughly evaluated in lung cancer. In this study, we investigated the distribution of ILCs and their subgroups throughout the lung tissue diseased region, non-diseased region, and peripheral blood of adult lung cancer patients. We further analyzed the differences between $NKp44^+$ and $NKp44^-$ ILC3s in the diseased and non-diseased regions by high-throughput RNA sequencing (RNA-seq).

Materials and methods

Patients and samples

Tissues of lung cancer regions and distal matched non-cancer regions were collected from patients with lung cancer who underwent surgical resection. Diseased and non-diseased regions were confirmed by pathological evaluation. Peripheral blood was also collected from the patients; however, in some cases, peripheral blood could not be obtained. None of the subjects underwent chemotherapy or radiotherapy before resection. Mononuclear cells were isolated from the peripheral blood samples of healthy donors, who were generally in good health without symptoms of infection for at least 1 week prior to sample collection. The samples were confirmed to be free from human immunodeficiency virus, hepatitis B virus, and hepatitis C virus infections. All samples were collected from patients who visited the First Hospital of Jilin University. Patient data are shown in Table S1.

Single-cell suspensions from lung tissue

Lung tissues were rinsed with cold phosphate-buffered saline (PBS) to remove residual blood, cut into small pieces (<3 mm), and incubated at 37 °C for 40 min in digestion medium containing RPMI 1640 media, collagenase IV (1 mg/mL, Roche, Basel, Switzerland), DNase (15 μg/mL, Sigma, St. Louis, MO, USA), 2 % fetal bovine serum, and 1 % penicillin/streptomycin. After digestion, the cells were filtered through a 70 μm filter and subjected to red blood cell lysis. Mononuclear cells were isolated from the blood samples using Ficoll-Paque Plus (GE Healthcare, Little Chalfont, UK).

Flow cytometry staining and analysis

For ILC staining, single-cell suspensions were stained with fluorescein isothiocyanate-conjugated lineage cocktail (Lin) (CD3, CD14, CD19, CD20, CD94, CD34, CD1a, CD11c, CD123, TCRα/β, TCRγ/δ, and FCR), BV605-conjugated CD117, phycoerythrin (PE Cy7)-conjugated CD294 (CRTH2), Percp-cy5.5-conjugated CD127, allophycocyanin (APC)-H7-conjugated CD45, PE-conjugated CCR6, PE-conjugated CCR7, PE-conjugated ICOS, PE-conjugated NKp30, PE-conjugated NKp46, live-dead stain (Aqua), and Fc block in PBS containing 0.5 % bovine serum albumin at 4 °C for 20 min. The cells were analyzed using the gating strategy shown in Figure 1a.

Cell sorting and RNA sequencing

Single cells were stained with Lin, PE/Cy7-conjugated CD294 (CRTH2), Percp-cy5.5-conjugated CD127, APC-H7-conjugated CD45, and Fc block in PBS containing 0.5 % bovine serum albumin at 4 °C for 20 min. The cells were sorted according to the gating strategy shown in Figure 1a. Sorted cells were collected in cell lysis buffer for RNA isolation and immediately stored in liquid nitrogen. The RNA from all samples was sequenced by the BGI Group (Guangdong, China).

Statistical analysis

Flow cytometry data were acquired with LSR Fortessa running DiVa software (BD Biosciences, Franklin Lakes, NJ, USA) and analyzed using FlowJo software (FlowJo, Ashland, OR, USA). To compare flow cytometry data among different groups, a *t*-test was performed, and

paired group data from the same patient were analyzed using a paired *t*-test. The relationships between ILCs and other immune cells were analyzed using a linear regression test. The associations between ILC subgroups and clinical data were determined using Fisher's exact test. Patient characteristics are expressed as the mean ± SD. Flow cytometric data are expressed as the mean ± SEM. All data analyses were performed using GraphPad Prism software (version 5.0; GraphPad, Inc., La Jolla, CA, USA). Statistical significance was set at $P < 0.05$.

RNA-seq for differentially expressed gene (DEG) analysis employed an R package to identify DEGs or isoforms for data from different samples; the detailed method was described by Wang et al. (2010).

Results

NKp44$^+$ ILC3s were more common in diseased than non-diseased regions in lung tissue and almost absent in the peripheral blood of patients with lung cancer

ILCs were initially identified as lineage-negative non-T and non-B cells without antigen recombinant gene expression; however, the surface antibodies present in this family remain controversial. In some previous studies, only T and B cells were removed, whereas others suggested that the purity of ILCs increased when a more rigorous gate marking strategy was used. There is currently no consensus regarding the definite phenotype of ILC1s, including intestinal endothelium ILC1s, cNK, CD127$^-$ ILC1s, and CD127$^+$ ILC1s. Thus, we focused on the distribution of CD127$^+$ ILCs: ILC1s, ILC2s, and ILC3s. LTi cells are difficult to separate based on their marker expression; therefore, LTi may be included in the ILC3 group, as previously reported (Carrega et al., 2015; Simoni et al., 2017). To ensure the purity of ILCs, we applied a strict lineage gating strategy based on previous reports (Bernink et al., 2013; Hazenberg and Spits, 2014; Mjosberg et al., 2011).

To determine the differences in ILCs between the lung cancer microenvironment and peripheral immune organs, we compared the distribution of ILCs in the diseased region, non-diseased region, and peripheral blood from the same patient. The percentage of ILCs/CD45$^+$ cells in the lung cancer region was 0.25 ± 0.03 %, which was higher than that in the peripheral blood (0.15 ± 0.02 %) ($P < 0.05$), whereas the lung cancer region and non-diseased region showed no significant difference (Figure 1b). Additionally, the absolute number of ILCs per gram in the lung cancer region was higher than that in the non-diseased region ($P < 0.01$) (Figure 1b),

whereas no significant difference in ILCs was observed between the peripheral blood samples from patients and healthy donors.

The %ILC1s/ILCs in the diseased region was significantly lower than in the non-diseased region ($P < 0.01$), whereas the %ILC1s/ILCs in the peripheral blood of lung cancer patients was 56.64 ± 3.49 %, which was significantly higher than in both the diseased and non-diseased regions ($P < 0.001$) (Figure 1c). Furthermore, there was also no significant difference in %ILC2s/ILCs among the diseased region, non-diseased region, and peripheral blood (Figure 1c). Additionally, the percentage of ILC3s/ILCs in the diseased region was 54.14 ± 2.80 %, which was significantly higher than that in the non-diseased region and peripheral blood (Figure 1c).

According to the expression of NKp44, ILC3s can be classified into NCR^- ILC3s ($NKp44^-$ ILC3s) and NCR^+ ILC3s ($NKp44^+$ ILC3s); therefore, we further analyzed the ILC3s by gating for NKp44 (Figure 1d). There was no significant difference in %$NKp44^-$ ILC3s/ILCs between diseased and non-diseased regions. The percentage of $NKp44^+$ ILC3s in ILCs was higher in diseased regions than non-diseased regions. Furthermore, only very low levels were detected in the peripheral blood (Figure 1e).

Transcriptional sequencing revealed that $NKp44^+$ and $NKp44^-$ ILC3s shared some general gene transcripts

To further compare $NKp44^-$ and $NKp44^+$ ILC3s, we determined the transcriptomic profiles of these two groups in the lung tissue of three patients with lung cancer by RNA-seq. We detected numerous genes, including known and novel genes, which are predicted coding transcripts that were previously unknown (Figure 2a). Figure 2b shows the gene expression number of different fragments per kilobase of transcript per million mapped reads (FPKM). We classified the gene expression number in three different FPKM ranges (FPKM ≤ 1, FPKM 1–10, and FPKM ≥ 10). FPKM value ≥ 10 was the highest expression level, whereas FPKM value ⩽ 1 indicated a low expression level.

Analysis of the basic characteristics of RNA transcript expression in $NKp44^+$ and $NKp44^-$ ILC3s in the diseased and non-diseased regions showed that *IL-7R* (CD127), *KLRB1* (CD161), and *ID2* were highly expressed. Moreover, *AHR* showed moderate expression and *NCR2* (NKp44) was nearly absent in $NKp44^-$ ILC3s, which was expected given that we had sorted

NKp44$^-$ ILC3s. Alternatively, in the non-diseased region, *NCR2* was expressed less than in the diseased region. *GATA3* and *RORC* were both expressed in the NKp44$^+$ and NKp44$^-$ ILC3 groups, whereas *TBX21* was not expressed in either group. *PTGDR2*, the CRTH2 transcript, was not expressed in ILC3s (Figure 2c).

Comparison of NKp44$^-$ and NKp44$^+$ ILC3s yielded numerous DEGs

Comparison of NKp44$^+$ and NKp44$^-$ ILC3s in the entire dataset revealed numerous DEGs. Compared with NKp44$^+$ ILC3s, NKp44$^-$ ILC3s had 10 860 DEGs, with 4926 upregulated genes and 5934 downregulated genes, whereas 19 429 genes were not differentially expressed (Figure 3b). Figure 3b shows the expression (log_2 fold-changes from their FPKM values) of some of the genes in the three samples. Upregulated and downregulated clusters, as well as genes without significant differential expression, can be observed in the figure.

Using DEGs, we performed Gene Ontology (GO) classification for biological process enrichment of the DEGs. We compared the biological processes of NKp44$^+$ and NKp44$^-$ ILC3s. Most DEGs were found to be related to cellular processes, biological regulation, metabolic processes, and response to stimuli (Figure 3b). Compared with in NKp44$^+$ ILC3s, more genes were downregulated in NKp44$^-$ ILC3s.

To analyze the function of NKp44$^+$ and NKp44$^-$ ILC3s, we performed DEG by Kyoto Encyclopedia of Genes and Genomes (KEGG) pathway classification and functional enrichment. The pathway classification contained cellular processes, environmental information processing, genetic information processing, human diseases, metabolism, and organismal systems. Here, we focused on their function in innate immunity in the lung cancer tumor environment; therefore, we analyzed the pathway with the most DEGs in the environmental information processing and immune system. There were 2852 DEGs in the signal transduction pathway and 982 DEGs in the signaling molecules and interaction pathway (Figure 3c).

In the signal transduction pathway, most DEGs were involved in the Ras, RAP1, Jak-STAT, TGF-β, Notch, NF-κB, and Toll-like receptor signaling pathways

In the signal transduction pathway, most DEGs were involved in the Ras, RAP1, Jak-STAT, TGF-β, Notch, NF-κB, and Toll-like receptor signaling pathways. In these pathways, the percentages of known DEGs with pathway annotation ranged from 2.00 % in the Ras pathway to

0.61 % in the Toll-like receptor signaling pathway (Figure 4a). Compared with in NKp44^{+} ILC3s, there were more downregulated genes in NKp44^{-} ILC3s for the Ras, RAP1, Jak-STAT, Notch, NF-κB, and Toll-like receptor signaling pathways, whereas there were more upregulated genes for the TGF-β signaling pathway (Figure 4b).

In the Ras pathway, *BAD*, *BCL2L1*, *CSF1*, *EFNA1*, *PLA2G4A*, *PLA2G16*, *VEGFA*, *FGF20*, and *LRRC57* transcripts were highly expressed in NKp44^{+} ILC3s, and higher than in NKp44^{-} ILC3s. (Figure 4c).

In the RAP1 pathway, *CSF1*, *EFNA1*, *VEGFA*, *ST7*, *FGF20*, *PLEKHA5*, and *ORAOV1* transcripts were highly expressed in NKp44^{+} ILC3s, higher than in NKp44^{-} ILC3s. *CDH1*, *ITGB3*, *MAPK13*, *MAPK12*, *PARD3*, and *FAM171A1* transcripts were more highly expressed in NKp44^{+} ILC3s. These genes are involved in cell adhesion, migration, polarity, proliferation, survival, and gene activation (Figure 4c).

In the Jak-STAT signaling pathway, *BCL2L1*, *TMEM50B*, *CDKN1A*, *CSF2*, *IL2RB*, *LIF*, *STAT3*, *OSMR*, *LEPROT*, and *IL23R* transcripts were highly expressed in NKp44^{+} ILC3s, higher than in NKp44^{-} ILC3s. (Figure 4c).

In the TGF-β signaling pathway, *CREBBP*, *E2F4*, *PPP2R1A*, *BAMBI*, and *CRIM1* were highly expressed in NKp44^{-} ILC3s, higher than in NKp44^{+} ILC3s. *BMPR1A*, *CRYBA4*, *CRYGS*, *EP300*, *IFNG*, *INHBA*, *TGFB1*, *UPK3A*, *NOG*, and *FSTL3*, transcripts were moderately expressed in NKp44^{-} ILC3s, higher than in NKp44^{+} ILC3s (Figure 4c).

In the Notch signaling pathway, *DTX3*, *APH-1*, *CPNE7*, *NCSTN*, *NUMB*, *TLE4*, *RBPJ*, *GRN*, *EP300*, *DVL3*, and *CREBBP* transcripts were moderately expressed in both NKp44^{-} and NKp44^{+} ILC3s. Compared with in NKp44^{+} ILC3s, gene transcripts including *APH-1*, *CPNE7*, *NUMB*, *RBPJ*, and *GRN 1* were downregulated in NKp44^{-} ILC3s (Figure 4c).

In the NF-κB pathway, *MAP3K7CL*, *LY96*, *TRADD*, *TRAF3*, *SYK*, *LTB*, *IL1B*, *ICAM1*, *CHUK*, and *BCL2L1* transcripts were moderately expressed in both NKp44^{-} and NKp44^{+} ILC3s. *BCL2L1*, *IKBKG*, *VCAM1*, *CXCL12*, *CCL19*, and *ICAM1*, which are involved in inflammation, immunity, cell survival, and other pathways, were upregulated in NKp44^{+} ILC3s (Figure 4c).

In the Toll-like receptor signaling pathway, the transcript levels of *CD40*, *CD80*, *CHUK*, *CTSK*, *FADD*, *IFNB1*, *IKBKE*, *IRF7*, *LBP*, *LY96*, *MAP3K7CL*, *MAPK12*, *MAPK13*, *PIK3R2*, *SPP1*, *TLR2*, *TLR3*, *TLR5*, *TLR6*, *TLR8*, *TMED7-TICAM2*, *TWF2*, and *WSCD2* were higher in NKp44^{+} than in NKp44^{-} ILC3s; *CD40*, *CTSK*, *IKBKE*, and *LY96* transcript levels in particular

were obviously increased (Figure 4c).

In the signaling molecules and interaction pathway, more DEGs were clustered in the cell adhesion molecules and cytokine-cytokine receptor interaction pathways

In the signaling molecules and interaction pathway, most DEGs were concentrated in the cell adhesion molecules and cytokine-cytokine receptor interaction pathways. The cell adhesion molecules pathway included 1.69 % of the total DEGs with pathway annotation (Figure 5a). Compared with NKp44^{+} ILC3s, NKp44^{-} ILC3s had 63 downregulated genes and 35 upregulated genes in the cell adhesion molecules pathway (Figure 5b). In the cytokine-cytokine receptor interaction pathway, 2.1 % of the DEGs were annotated with pathway annotation (Figure 5a). Compared with NKp44^{+} ILC3s, NKp44^{-} ILC3s had 74 upregulated genes and 48 upregulated genes in this pathway (Figure 5b).

CSF1, *CSF2*, *LIF*, *TNFSF13*, *TNFSF4*, *VEGFA*, *IL1B*, *IL23A*, and *LTB* transcripts were highly expressed in both NKp44^{-} and NKp44^{+} ILC3s, whereas *CSF1*, *CSF2*, *LIF*, *LTB*, *TNFSF13*, *TNFSF4*, and *VEGFA* transcript levels were higher in NKp44^{+} ILC3s. *IL1B* and *IL23A* transcript levels were higher in NKp44^{-} ILC3s. *IL22* and *TGFB1* transcripts were moderately expressed in NKp44^{-} ILC3s and were higher than in NKp44^{+} ILC3s. *IL17C* transcripts were moderately expressed in NKp44^{+} ILC3s and were higher than in NKp44^{-} ILC3s (Figure 5c).

CCL5, *CCL7*, *CCL19*, *CCL20*, *CXCL9*, *CXCL12*, and *CXCL1*3 transcript levels were higher in NKp44^{+} ILC3s. Among these genes, *CCL5* and *CCL20* transcripts were highly expressed. *CCL3*, *CCL13*, and *CCL14* transcript levels were higher in NKp44^{-} ILC3s (Figure 5c).

HLA, including *HLA-DQA1*, *HLA-DQB1*, *HLA-DRB1*, *HLA-DRB3*, and *HLA-DRB5*, was highly expressed in both NKp44^{-} and NKp44^{+} ILC3s, with higher expression levels in NKp44^{+} ILC3s. *HLA-DOB* and *HLA-DQB2* transcripts had moderate expression in NKp44^{+} ILC3s and low expression in NKp44^{+} ILC3s (Figure 5c).

CD2, *CD40*, *ICAM1*, *ITGAV*, *LEPROT*, *ITGAM*, *LRRC70*, *MPZL2*, *SDC4*, *SELL*, *SELPLG*, and *ICOS* were highly expressed in NKp44^{-} and NKp44^{+} ILC3s, with higher expression of *CD2*, *CD40*, *ICAM1*, *LEPROT*, *MPZL2*, and *SDC4* in NKp44^{+} ILC3s. Expression of *SDC1*, *SELL*, *SELPLG*, *ITGAM*, and *LRRC70* was higher in NKp44^{-} ILC3s. *CD276*, *CD80*, *CTLA4*, *ICOSL*, and *VCAM1* had moderate expression in NKp44^{+} ILC3s and low expression in NKp44^{-} ILC3s

(Figure 5c).

Discussion

The tissue microenvironment is vital for the development and differentiation of ILCs. ILC progenitors reportedly seed themselves into tissues in both the embryonic and adult phases and undergo further development and differentiation in the tissue microenvironment (Bando et al., 2015; E et al., 2014; Vivier et al., 2018). ILC3s are the dominant group in the colon, lymph nodes, and spleen (Yudanin et al., 2019). Our findings showed that ILC3s were also the dominant group in the lung, which is consistent with the former report (Carrega et al., 2015).

ILC3s exhibit a high degree of heterogeneity and express varying levels of surface markers. According to NKp44, ILC3s can be classified into NKp44$^-$ and NKp44$^+$ ILC3s. NKp44$^-$ ILC3s have multi-differentiation potential and can differentiate into NKp44$^+$ ILC3s *in vitro* (Lim et al., 2017). Our findings show that in lung cancer, the number of NKp44$^+$ ILC3s is increased in the diseased region. Carrega et al. (2015) suggested that tumor NCR$^+$ ILC3s interact with both lung tumor cells and tumor-associated fibroblasts by binding to the NKp44 receptor, resulting in cytokine release(Carrega et al., 2015). The increase in NKp44$^+$ ILC3s may play a role in the cancer immunity cycle in lung cancer. The shift from NKp44$^-$ to NKp44$^+$ ILC3s evoked our interest. Therefore, we used RNA-seq to compare NKp44$^-$ and NKp44$^+$ ILC3s in lung cancer tissues to reveal their characteristics.

Transcript sequencing revealed that NKp44$^-$ and NKp44$^+$ ILC3s shared some general gene transcripts. Both expressed *ID2*, *GATA3*, and *AHR* transcripts, which are necessary factors for ILC development, similar to reports on human peripheral blood and tonsils (Bjorklund et al., 2016; Lim et al., 2017; Simoni et al., 2017). Both cell types expressed *RORc*, but not *TBOX21*. Additionally, they did not express *CRTH2* transcripts. These results are consistent with those of previous studies in human peripheral blood, tonsils, spleens, and small intestines (Bjorklund et al., 2016; Lim et al., 2017; Simoni et al., 2017; Yudanin et al., 2019). NKp44$^+$ and NKp44$^-$ ILC3s highly expressed transcripts including *IL2R* and *IL7R*, which are essential for ILC survival.

Between NKp44$^-$ with NKp44$^+$ ILC3s, the signal transduction pathway had the greatest number of DEGs. In the Ras signaling pathway, P13K, IKK, BAD, and BCL-x, which are related to cell survival, growth, and migration, were upregulated in NKp44$^+$ ILC3s. In the RAP1

pathway, talin, integrin, PAR3, Cad, and p38MAPK were upregulated in NKp44^{+} ILC3s. These molecules are related to cell adhesion, migration, and proliferation. These signaling pathways may enhance the biological function of NKp44^{+} ILC3s in lung cancer.

The signal transduction pathway influences ILC3 phenotype transformation. Notch signaling contributes to the transition of NCR (−) cells into NCR (+) cells, which are the more proinflammatory subset (Chea et al., 2016; Viant et al., 2016). TGF-β signaling impairs the generation of NCR^{+} ILC3s *in vivo* (Viant et al., 2016). Our results show that key molecules in the Notch signaling pathway are more abundant in NKp44^{+} than NKp44^{-} ILC3s, whereas the TGF-β signaling pathway is downregulated in NKp44^{+} ILC3s. This result is consistent with the hypothesis that the plasticity of ILC3s is regulated by the balance between the opposing effects of Notch and TGF-β signaling (Viant et al., 2016).

In the JAK-STAT signaling pathway, the activation of STAT3 is a key event in promoting ILC3 functions and is related to the production of IL-17 and IL-22 (Guo et al., 2014; Rankin et al., 2016). In our results, STAT3 was upregulated in NKp44^{+} ILC3s compared with in NKp44^{-} ILC3s. *Il17* transcript levels were higher in NKp44^{+} ILC3s than in NKp44^{-} ILC3s, whereas *Il22* transcript levels were lower in NKp44^{+} ILC3s. In previous reports, tonsil NKp44^{+} ILC3s were shown to produce more IL-22 than NKp44^{-} ILC3s *in vitro* after stimulation(Crellin et al., 2010; Hoorweg et al., 2012). Single-cell RNA sequencing of tonsil ILCs revealed that *Il22* transcript expression in ILC3s was low (Bjorklund et al., 2016). Our results reflect the resting state of ILC3s in the tumor microenvironment without any in vitro stimulation. The reason for the lower IL-22 and higher IL-17 transcript levels in NKp44^{+} ILC3s in lung cancer requires further analysis.

In the NF-κB pathway, our results showed that levels of adhesion molecules (ICAM-1 and VCAM-1) were higher in NKp44^{+} ILC3s, which enhanced lymphocyte adhesion, T cell co-stimulation, and inflammation. The NF-κB pathway enhances the levels of growth factors (GM-CSF, G-CSF, and M-CSF). NKp44^{+} ILC3s expressed high levels of CSF1 and CSF2, which play essential roles in the regulation of survival, proliferation, and differentiation of hematopoietic precursor cells, especially mononuclear phagocytes, such as macrophages and monocytes. In addition, chemokine levels were increased in NKp44^{+} ILC3s in lung cancer and enhanced the infiltration of immune cells. Therefore, NKp44^{+} ILC3s may play an important role in innate immunity and inflammatory processes.

Previous reports have shown that ILCs express TLR2, TLR3, and TLR9. TLR3 increases ILC synthesis of TNF-α (Marafini et al., 2015). TLR2 signaling induces LTi-like ILC production by IL-5, IL-13, and IL-22 (Crellin et al., 2010). More upregulated molecular transcripts of the Toll-like receptor signaling pathway were detected in NKp44^{+} ILC3s than in NKp44^{-} ILC3s. TLR2 and TLR5 transcript expression was higher in NKp44^{+} ILC3s. The Toll-like receptor signaling pathway activated in NKp44^{+} ILC3s may mediate the production of downstream cytokines, which are involved in the early immune defense.

MHCII is expressed in ILC2s and ILC3s. Human ILC2s express MHCII and present antigens to T cells (Oliphant et al., 2014). ILC3s maintain intestinal homeostasis through MHCII-dependent interactions with CD4^{+} T cells that limit pathogenic adaptive immune cell responses to commensal bacteria (Hepworth et al., 2013). MHCII transcript levels were higher in NKp44^{+} than in NKp44^{-} ILC3s. MHCII participates in antigen presentation and may link innate and acquired immunity in lung cancer.

The expression of cell adhesion molecules, including CD40, ICOS, ICOSL, and CD80, was higher in NKp44^{+} ILC3s in lung cancer. CD40 can upregulate co-stimulatory molecules, activate antigen-presenting cells (APCs), and influence T cell functions (Xu and Song, 2004). ILC2s overexpress ICOS and promote ILC2 activation and amplification in the lungs (Kamachi et al., 2015). Additionally, the ICOS-ICOSL interaction on ILC2s activates the STAT5 signaling pathway on ILC2s to maintain cell survival (Maazi et al., 2015). Elevated levels of ICOS and CD40 molecules activate the function of NKp44^{+} ILC3s. CD80 and ICOSL are expressed on APCs and bind to T cell receptors to regulate their immune response (Peach et al., 1995; Yoshinaga et al., 2000). Elevated CD80 and ICOSL may enable NKp44^{+} ILC3s to modulate T cell function.

CD276 and CTLA4 are important checkpoints that regulate immune cell activity and antitumor immunity. Expression of both *CD276* and *CTLA4* was upregulated in NKp44^{+} ILC3s compared with in NKp44^{-} ILC3s, indicating that NKp44^{+} ILC3 activity may be downregulated by these molecules. Thus, blocking CD96, CD276, and CTLA4 activity may be an effective method for activating ILC3s.

In summary, the number of NKp44^{+} ILC3s is increased in the diseased regions of lung cancer. In transcript-level analysis, NKp44^{+} and NKp44^{-} ILC3s were generally similar, while numerous DEGs were found between these two subgroups. In the signal transduction pathway

and signaling molecules and interaction pathway, more genes were upregulated in NKp44^{+} ILC3s. These pathways are related to survival, proliferation, activation, interleukin production, and antigen presentation. To the best of our knowledge, this is the first study has provided the transcript landscape of DEGs in NKp44^{+} and NKp44^{-} ILC3s in lung cancer. Our results provided a theoretical basis for further ILC3 studies which will potentially useful in developing therapies. One limitation of this study is that the results are at the transcript level, and the roles of ILC3s in lung cancer must be further studied by functional analysis in either a human or mouse model.

Declarations

Funding

This work was supported by the National Natural Science Foundation of China (Grant Nos. 81571534, 81800021, and 81901591), the Scientific and Technological Developing Plan of Jilin Province (Grant Nos. 20200201588JC, 20200201464JC).

Competing interests

The authors have declared that no conflict of interest exists.

Availability of data and material

The datasets relevant to the current study are available from the corresponding author on reasonable request.

Authors' contributions

JTC and HC conceived the study. HC, SZ, JW, and GXZ performed the experiments and analyzed the data. CYJ and ZGY recruited patients and curated the patient samples and information. XPL and TTL contributed to the flow cytometric studies. HC and BG generated and analyzed RNA-seq data. JTC conceived and designed the experiments and supervised the work with participation from JWC, HU, and YJL. All authors contributed to the data analysis, reviewed, and edited the manuscript.

Ethics approval

This study was approved by the Ethics Committee of the First Hospital of Jilin University (2015-

051).

Consent to participate

Written informed consent was obtained from each patient and healthy donor. This study was conducted in accordance with the Declaration of Helsinki.

Figure legends

Figure 1 Group 3 innate lymphoid cells (ILC3s) were predominant in lung cancer tissues, with particularly high levels of NKp44$^+$ ILC3s in diseased regions. Lung tissue was collected from patients with lung cancer, containing both lung tissues of the diseased region (LC) and distal matched non-diseased region (LC-DM). Peripheral blood (PB) was collected from the same patients. PB was also collected from healthy donors (HD). **a**. Gating strategy of ILCs and ILC1–3s by flow cytometry. **b**. ILC proportion in CD45$^+$ cells in LC, LC-DM, and LC-PB; ILC proportion per gram of LC and LC-DM; and numbers of ILCs per mL of LC-PB and HD-PB. **c**. Proportion of ILC1–3s in total ILCs of LC, LC-DM, and LC-PB; **d**. Expression of NKp44 on ILC1–3s was quantified by flow cytometry. **e**. Proportion of NKp44$^-$ and NKp44$^+$ ILC3s in total ILCs of LC, LC-DM, and LC-PB. Lung cancer tissue, n = 42; PB of lung cancer, n = 26. Each point represents one donor

Figure 2 NKp44$^+$ and NKp44$^-$ group 3 innate lymphoid cells (ILC3s) shared some general gene transcripts based on transcriptional sequencing analysis. NKp44$^+$ and NKp44$^-$ ILC3s were sorted from diseased regions of lung cancer, and RNA sequencing analysis was performed. **a**. List of generally known and novel genes of three samples in diseased and non-diseased regions. Novel genes were defined as those with predicted coding transcripts that were previously unknown. **b**. Distribution of gene expression. The Y-axis shows the average $\log_{10}$ fragments per kilobase of transcript per million mapped reads (FPKM) value of three samples. **c**. Transcript expression of *IL-7R*, *KLRB1*, *ID2*, *CD117*, *AHR*, *NCR2*, *PTGDR2*, *TBX21*, *GATA3*, and *RORC*

Figure 3 RNA-seq analysis revealed numerous differentially expressed genes (DEGs)

between NKp44$^+$ and NKp44$^-$ group 3 innate lymphoid cells. a. Volcano plot of DEGs: the X-axis shows $\log_2$-transformed fold-change, and the Y-axis shows $-\log_{10}$-transformed significance. Red points represent upregulated DEGs. Blue points represent downregulated DEGs. Gray points represent non-DEGs. **b**. GO classification of upregulated and downregulated genes. The Y-axis shows GO terms. The X-axis shows the number of up/downregulated genes. **c**. The X-axis shows the number of DEGs. The Y-axis shows KEGG functional classifications. There are seven branches for KEGG pathways: cellular processes, environmental information processing, genetic information processing, human disease, metabolism, and organismal systems

Figure 4 Most differentially expressed genes (DEGs) were in the signal transduction pathway, and DEGs tended to be upregulated in NKp44$^+$ group 3 innate lymphoid cells (ILC3s). a. Percentages of DEGs in the top seven signal transduction pathways. The Y-axis shows the percentages of DEGs out of total genes in the KEGG pathways. The X-axis shows KEGG pathways. **b**. Comparing with NKp44$^+$ ILC3s, the numbers of downregulated (blue) and upregulated genes (red) are shown for NKp44$^-$ ILC3s. The Y-axis shows the number of DEGs. The X-axis shows the KEGG pathways. **c**. Hierarchical clustering heatmaps of KEGG pathways depicting differential expression between NKp44$^+$ and NKp44$^-$ ILC3s in the diseased and non-diseased regions from three patients with lung cancer. Gene expression changes ($\log_2$ fold-changes from their fragments per kilobase of transcript per million mapped reads values) are represented from lowest to highest as blue to red in the heat map; grey indicates that no gene transcript was detected.

Figure 5 In the signaling molecules and interaction pathway, more differentially expressed genes (DEGs) were clustered in the cell adhesion molecules and cytokine-cytokine receptor interaction pathways. a. Percentages of DEGs in the cell adhesion molecules and cytokine-cytokine receptor interaction pathways. The Y-axis shows the percentages of DEGs out of total genes in the KEGG pathways. The X-axis shows the KEGG pathways. **b**. Comparing with NKp44$^+$ group 3 innate lymphoid cells (ILC3s), the numbers of downregulated (blue) and upregulated genes (red) are shown for NKp44$^-$ ILC3s. The Y-axis shows the number of DEGs. The X-axis shows the KEGG pathways. **c**. Hierarchical clustering heatmaps of KEGG pathways depicting differential expression between NKp44$^+$ and NKp44$^-$ ILC3s in the diseased and non-

diseased regions from three patients with lung cancer. Gene expression changes (log_2 fold-changes from their fragments per kilobase of transcript per million mapped reads values) are represented from lowest to highest as blue to red in the heat map; grey indicates that no gene transcript was detected.

Supplementary information

Table S1. Sample information

Table S2. List of antibodies for ILCs

References

Bando, J.K., Liang, H.E., and Locksley, R.M. (2015). Identification and distribution of developing innate lymphoid cells in the fetal mouse intestine. Nature immunology *16*, 153-160.

Bernink, J.H., Peters, C.P., Munneke, M., te Velde, A.A., Meijer, S.L., Weijer, K., Hreggvidsdottir, H.S., Heinsbroek, S.E., Legrand, N., Buskens, C.J.*, et al.* (2013). Human type 1 innate lymphoid cells accumulate in inflamed mucosal tissues. Nature immunology *14*, 221-229.

Bjorklund, A.K., Forkel, M., Picelli, S., Konya, V., Theorell, J., Friberg, D., Sandberg, R., and Mjosberg, J. (2016). The heterogeneity of human CD127(+) innate lymphoid cells revealed by single-cell RNA sequencing. Nature immunology *17*, 451-460.

Carrega, P., Loiacono, F., Di Carlo, E., Scaramuccia, A., Mora, M., Conte, R., Benelli, R., Spaggiari, G.M., Cantoni, C., Campana, S.*, et al.* (2015). NCR(+)ILC3 concentrate in human lung cancer and associate with intratumoral lymphoid structures. Nat Commun *6*, 8280.

Chea, S., Perchet, T., Petit, M., Verrier, T., Guy-Grand, D., Banchi, E.G., Vosshenrich, C., Santo, J., Cumano, A., and Golub, R. (2016). Notch signaling in group 3 innate lymphoid cells modulates their plasticity. Science signaling *9*, ra45-ra45.

Cong, J., and Wei, H. (2019). Natural Killer Cells in the Lungs. Frontiers in immunology *10*, 1416.

Crellin, N.K., Trifari, S., Kaplan, C.D., Satoh-Takayama, N., and Spits, H. (2010). Regulation of Cytokine Secretion in Human CD127(+) LTi-like Innate Lymphoid Cells by Toll-like Receptor 2. Immunity *33*, 752-764.

E, M., LG, T.-A., T, G., P, D., U, S., W, H., M, B., D, P., K, S., and J, G. (2014). Human RORγt(+)CD34(+) cells are lineage-specified progenitors of group 3 RORγt(+) innate lymphoid cells. Immunity *41*, 988-1000.

Eberl, G., Colonna, M., Di Santo, J.P., and McKenzie, A.N. (2015). Innate lymphoid cells. Innate lymphoid cells: a new paradigm in immunology. Science *348*, aaa6566.

Guo, X., Qiu, J., Tu, T., Yang, X., Deng, L., Anders, R., Zhou, L., and Fu, Y.X. (2014). Induction of innate lymphoid cell-derived interleukin-22 by the transcription factor STAT3 mediates protection against intestinal infection. Immunity *40*, 25-39.

Hams, E., Armstrong, M.E., Barlow, J.L., Saunders, S.P., Schwartz, C., Cooke, G., Fahy, R.J., Crotty, T.B., Hirani, N., Flynn, R.J.*, et al.* (2014). IL-25 and type 2 innate lymphoid cells induce pulmonary fibrosis. Proceedings of the National Academy of Sciences of the United States of America *111*, 367-372.

Hazenberg, M.D., and Spits, H. (2014). Human innate lymphoid cells. Blood *124*, 700-709.

Hepworth, M.R., Monticelli, L.A., Fung, T.C., Ziegler, C.G., Grunberg, S., Sinha, R., Mantegazza, A.R., Ma, H.L., Crawford, A., Angelosanto, J.M.*, et al.* (2013). Innate lymphoid cells regulate CD4+ T-cell responses to intestinal commensal bacteria. Nature *498*, 113-117.

Hoorweg, K., Peters, C.P., Cornelissen, F., Aparicio-Domingo, P., Papazian, N., Kazemier, G., Mjosberg, J.M., Spits, H., and Cupedo, T. (2012). Functional Differences between Human NKp44(-) and NKp44(+) RORC(+) Innate Lymphoid

Cells. Frontiers in immunology *3*, 72.
Kamachi, F., Isshiki, T., Harada, N., Akiba, H., and Miyake, S. (2015). ICOS promotes group 2 innate lymphoid cell activation in lungs. Biochemical and biophysical research communications *463*, 739-745.
Kim, H.Y., Lee, H.J., Chang, Y.J., Pichavant, M., Shore, S.A., Fitzgerald, K.A., Iwakura, Y., Israel, E., Bolger, K., Faul, J.*, et al.* (2014). Interleukin-17-producing innate lymphoid cells and the NLRP3 inflammasome facilitate obesity-associated airway hyperreactivity. Nature medicine *20*, 54-61.
Lai, D.M., Shu, Q., and Fan, J. (2016). The origin and role of innate lymphoid cells in the lung. Military Medical Research *3*, 25.
Lim, A.I., Li, Y., Lopez-Lastra, S., Stadhouders, R., Paul, F., Casrouge, A., Serafini, N., Puel, A., Bustamante, J., Surace, L.*, et al.* (2017). Systemic Human ILC Precursors Provide a Substrate for Tissue ILC Differentiation. Cell *168*, 1086-1100 e1010.
Maazi, H., Patel, N., Sankaranarayanan, I., Suzuki, Y., Rigas, D., Soroosh, P., Freeman, G.J., Sharpe, A.H., and Akbari, O. (2015). ICOS:ICOS-ligand interaction is required for type 2 innate lymphoid cell function, homeostasis, and induction of airway hyperreactivity. Immunity *42*, 538-551.
Maizels, R.M., Hewitson, J.P., and Smith, K.A. (2012). Susceptibility and immunity to helminth parasites. Current opinion in immunology *24*, 459-466.
Marafini, I., Monteleone, I., Fusco, D.D., Cupi, M.L., Paoluzi, O.A., Colantoni, A., Ortenzi, A., Izzo, R., Vita, S., and Luca, E.D. (2015). TNF-α Producing Innate Lymphoid Cells (ILCs) Are Increased in Active Celiac Disease and Contribute to Promote Intestinal Atrophy in Mice. PloS one *10*.
Mjosberg, J.M., Trifari, S., Crellin, N.K., Peters, C.P., van Drunen, C.M., Piet, B., Fokkens, W.J., Cupedo, T., and Spits, H. (2011). Human IL-25- and IL-33-responsive type 2 innate lymphoid cells are defined by expression of CRTH2 and CD161. Nature immunology *12*, 1055-1062.
Monticelli, L.A., Sonnenberg, G.F., Abt, M.C., Alenghat, T., Ziegler, C.G., Doering, T.A., Angelosanto, J.M., Laidlaw, B.J., Yang, C.Y., Sathaliyawala, T.*, et al.* (2011). Innate lymphoid cells promote lung-tissue homeostasis after infection with influenza virus. Nature immunology *12*, 1045-1054.
Oliphant, C.J., Hwang, Y.Y., Walker, J.A., Salimi, M., Wong, S.H., Brewer, J.M., Englezakis, A., Barlow, J.L., Hams, E., Scanlon, S.T.*, et al.* (2014). MHCII-mediated dialog between group 2 innate lymphoid cells and CD4(+) T cells potentiates type 2 immunity and promotes parasitic helminth expulsion. Immunity *41*, 283-295.
Peach, R.J., Bajorath, J., Naemura, J., Leytze, G., Greene, J., Aruffo, A., and Linsley, P.S. (1995). Both Extracellular Immunoglobin-like Domains of CD80 Contain Residues Critical for Binding T Cell Surface Receptors CTLA-4 and CD28. Journal of Biological Chemistry *270*, 21181-21187.
Rankin, L.C., Girard-Madoux, M., Seillet, C., Mielke, L.A., Kerdiles, Y., Fenis, A., Wieduwild, E., Putoczki, T., Mondot, S., and Lantz, O. (2016). Complementarity and redundancy of IL-22-producing innate lymphoid cells. Nature immunology.
Scanlon, S.T., and McKenzie, A.N. (2012). Type 2 innate lymphoid cells: new players in asthma and allergy. Current opinion in immunology *24*, 707-712.
Silver, J.S., Kearley, J., Copenhaver, A.M., Sanden, C., Mori, M., Yu, L., Pritchard, G.H., Berlin, A.A., Hunter, C.A., Bowler, R.*, et al.* (2016). Inflammatory triggers associated with exacerbations of COPD orchestrate plasticity of group 2 innate lymphoid cells in the lungs. Nat Immunol *17*, 626-635.
Simoni, Y., Fehlings, M., Kloverpris, H.N., McGovern, N., Koo, S.L., Loh, C.Y., Lim, S., Kurioka, A., Fergusson, J.R., Tang, C.L.*, et al.* (2017). Human Innate Lymphoid Cell Subsets Possess Tissue-Type Based Heterogeneity in Phenotype and Frequency. Immunity *46*, 148-161.
Spits, H., Artis, D., Colonna, M., Diefenbach, A., Di Santo, J.P., Eberl, G., Koyasu, S., Locksley, R.M., McKenzie, A.N., Mebius, R.E.*, et al.* (2013). Innate lymphoid cells--a proposal for uniform nomenclature. Nature reviews Immunology *13*, 145-149.
Spits, H., and Cupedo, T. (2012). Innate lymphoid cells: emerging insights in development, lineage relationships, and function. Annual review of immunology *30*, 647-675.
Van Maele, L., Carnoy, C., Cayet, D., Ivanov, S., Porte, R., Deruy, E., Chabalgoity, J.A., Renauld, J.C., Eberl, G., Benecke, A.G.*, et al.* (2014). Activation of Type 3 innate lymphoid cells and interleukin 22 secretion in the lungs during Streptococcus pneumoniae infection. The Journal of infectious diseases *210*, 493-503.
Viant, C., Rankin, L.C., Girard-Madoux, M., Seillet, C., Shi, W., Smyth, M.J., Bartholin, L., Walzer, T., Huntington, N.D., and Vivier, E. (2016). Transforming growth factor- and Notch ligands act as opposing environmental cues in regulating the plasticity of type 3 innate lymphoid cells. Science signaling *9*, ra46.

Vivier, E., Artis, D., Colonna, M., Diefenbach, A., Di Santo, J.P., Eberl, G., Koyasu, S., Locksley, R.M., McKenzie, A.N.J., Mebius, R.E*., et al.* (2018). Innate Lymphoid Cells: 10 Years On. Cell *174*, 1054-1066.
Wang, L., Feng, Z., Wang, X., Wang, X., and Zhang, X. (2010). DEGseq: an R package for identifying differentially expressed genes from RNA-seq data. Bioinformatics *26*, 136-138.
Wohlfahrt, T., Usherenko, S., Englbrecht, M., Dees, C., Weber, S., Beyer, C., Gelse, K., Distler, O., Schett, G., Distler, J.H*., et al.* (2016). Type 2 innate lymphoid cell counts are increased in patients with systemic sclerosis and correlate with the extent of fibrosis. Annals of the rheumatic diseases *75*, 623-626.
Xu, Y., and Song, G. (2004). The role of CD40-CD154 interaction in cell immunoregulation.
Yoshinaga, S.K., Zhang, M., Pistillo, J., Horan, T., Khare, S.D., Miner, K., Sonnenberg, M., Boone, T., Brankow, D., Dai, T*., et al.* (2000). Characterization of a new human B7-related protein: B7RP-1 is the ligand to the co-stimulatory protein ICOS. International immunology *12*, 1439-1447.
Yudanin, N.A., Schmitz, F., Flamar, A.L., Thome, J.J.C., Tait Wojno, E., Moeller, J.B., Schirmer, M., Latorre, I.J., Xavier, R.J., Farber, D.L*., et al.* (2019). Spatial and Temporal Mapping of Human Innate Lymphoid Cells Reveals Elements of Tissue Specificity. Immunity *50*, 505-519 e504.

Figures

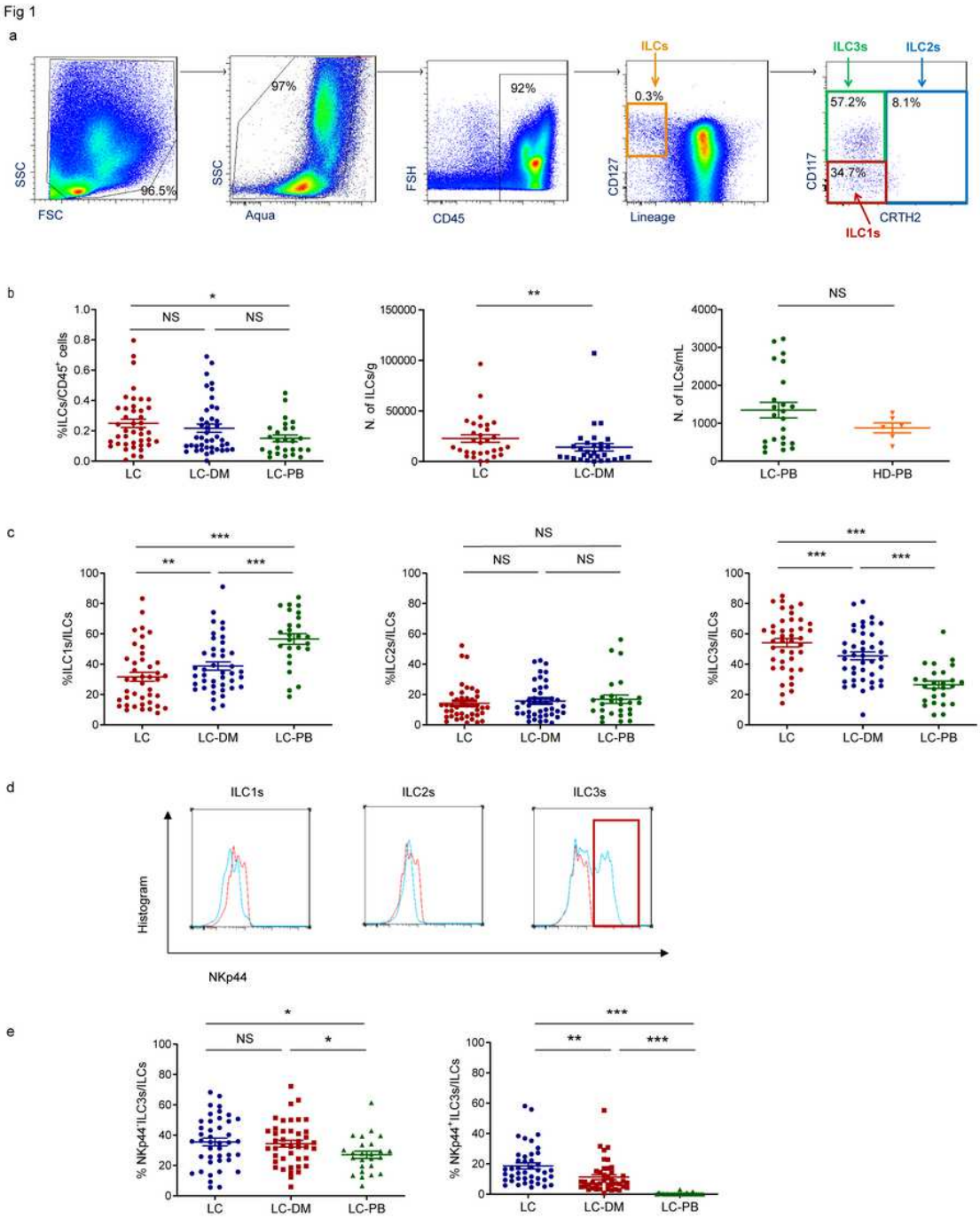

Figure 1

Group 3 innate lymphoid cells (ILC3s) were predominant in lung cancer tissues, with particularly high levels of NKp44+ ILC3s in diseased regions. Lung tissue was collected from patients with lung cancer, containing both lung tissues of the diseased region (LC) and distal matched non-diseased region (LC-DM). Peripheral blood (PB) was collected from the same patients. PB was also collected from healthy donors (HD). a. Gating strategy of ILCs and ILC1–3s by flow cytometry. b. ILC proportion in CD45+ cells in

LC, LC-DM, and LC-PB; ILC proportion per gram of LC and LC-DM; and numbers of ILCs per mL of LC-PB and HD-PB. c. Proportion of ILC1–3s in total ILCs of LC, LC-DM, and LC-PB; d. Expression of NKp44 on ILC1–3s was quantified by flow cytometry. e. Proportion of NKp44− and NKp44+ ILC3s in total ILCs of LC, LC-DM, and LC-PB. Lung cancer tissue, n = 42; PB of lung cancer, n = 26. Each point represents one donor

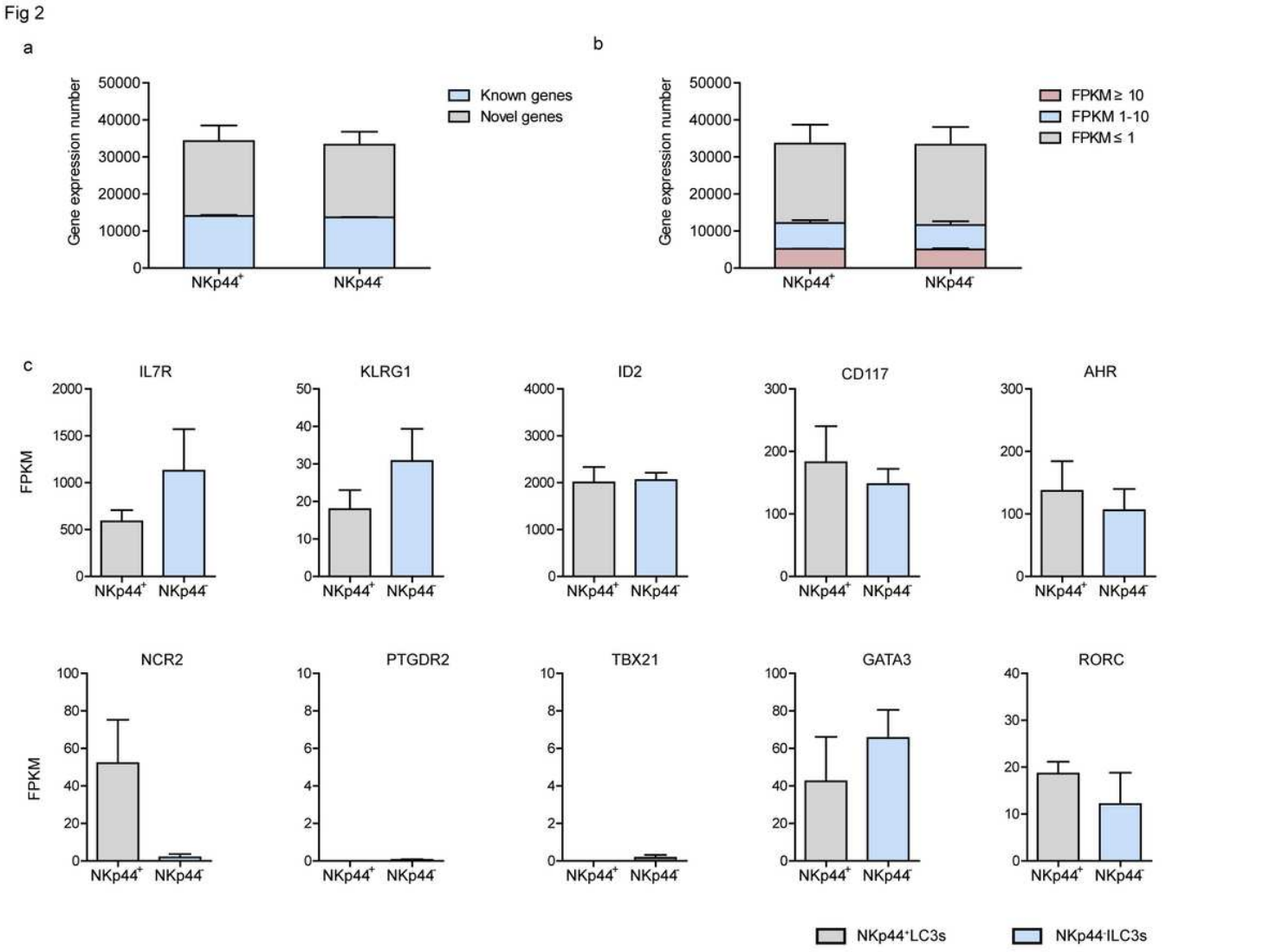

Figure 2

NKp44+ and NKp44− group 3 innate lymphoid cells (ILC3s) shared some general gene transcripts based on transcriptional sequencing analysis. NKp44+ and NKp44− ILC3s were sorted from diseased regions of lung cancer, and RNA sequencing analysis was performed. a. List of generally known and novel genes of three samples in diseased and non-diseased regions. Novel genes were defined as those with predicted coding transcripts that were previously unknown. b. Distribution of gene expression. The Y-axis shows the average log10 fragments per kilobase of transcript per million mapped reads (FPKM) value of three samples. c. Transcript expression of IL-7R, KLRB1, ID2, CD117, AHR, NCR2, PTGDR2, TBX21, GATA3, and RORC

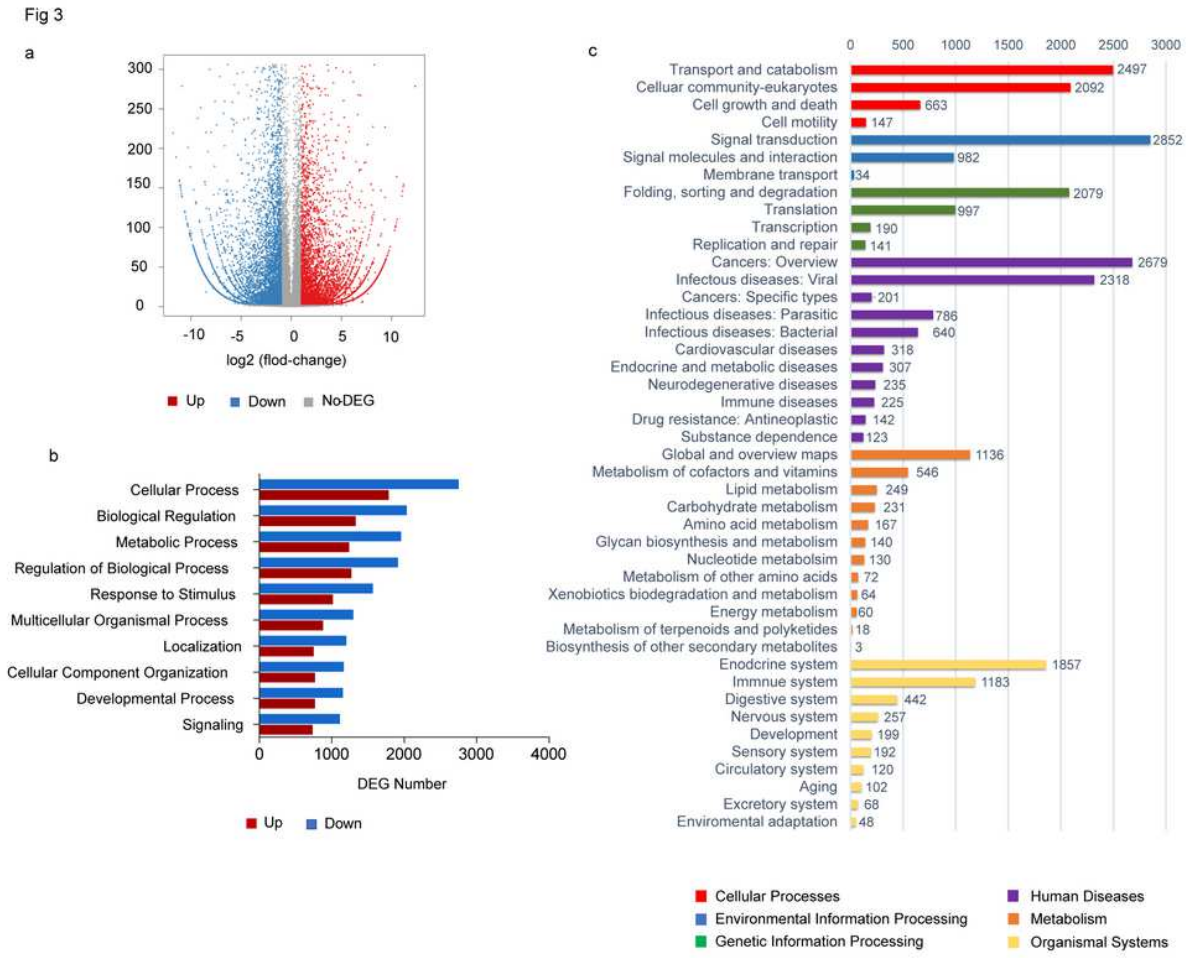

Figure 3

RNA-seq analysis revealed numerous differentially expressed genes (DEGs) 15 between NKp44+ and NKp44− group 3 innate lymphoid cells. a. Volcano plot of DEGs: the X-axis shows log2-transformed fold-change, and the Y-axis shows −log10-transformed significance. Red points represent upregulated DEGs. Blue points represent downregulated DEGs. Gray points represent non-DEGs. b. GO classification of upregulated and downregulated genes. The Y-axis shows GO terms. The X-axis shows the number of up/downregulated genes. c. The X-axis shows the number of DEGs. The Y-axis shows KEGG functional classifications. There are seven branches for KEGG pathways: cellular processes, environmental information processing, genetic information processing, human disease, metabolism, and organismal systems

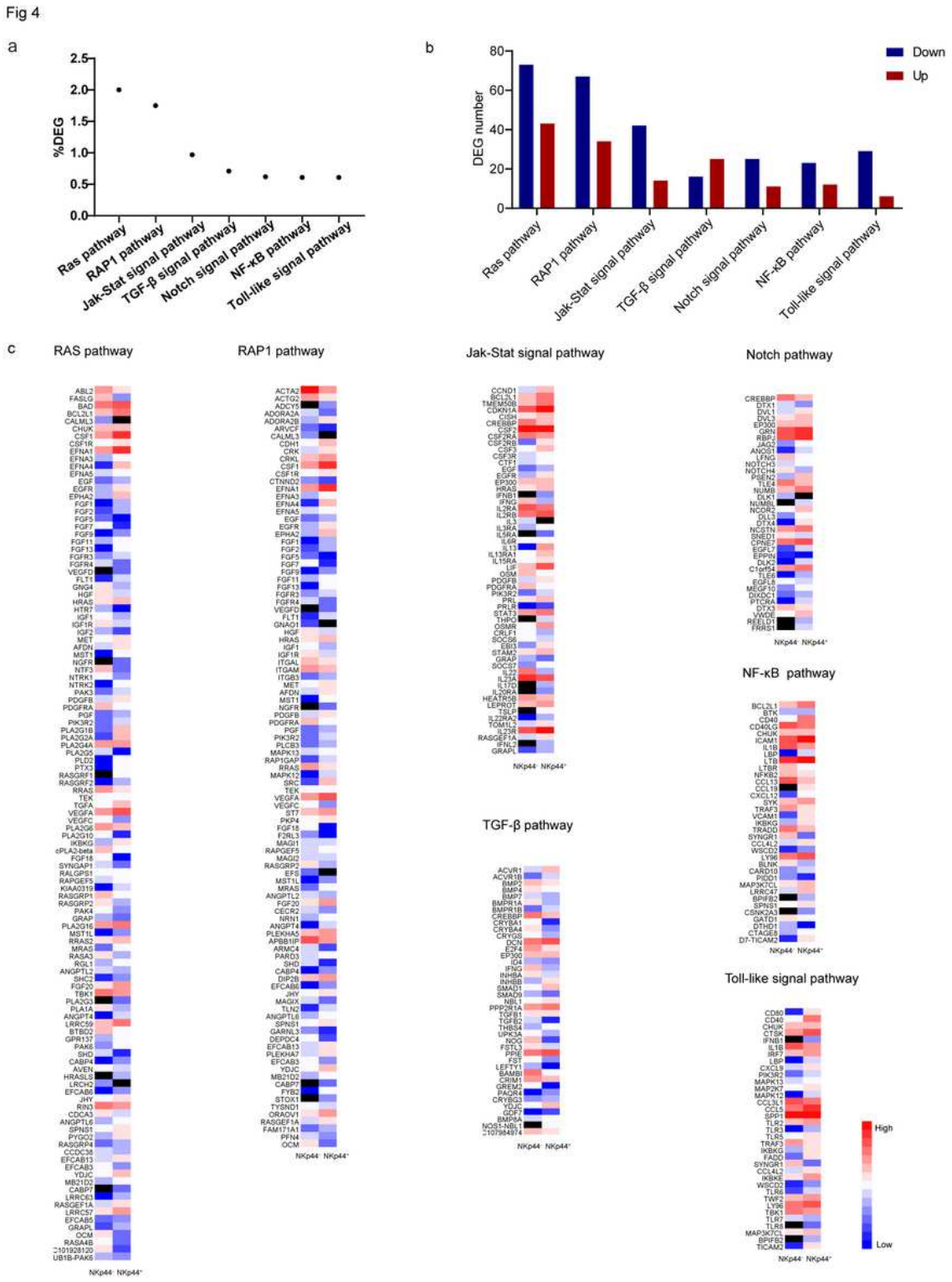

Figure 4

Most differentially expressed genes (DEGs) were in the signal transduction pathway, and DEGs tended to be upregulated in NKp44+ group 3 innate lymphoid cells (ILC3s). a. Percentages of DEGs in the top seven signal transduction pathways. The Y-axis shows the percentages of DEGs out of total genes in the KEGG pathways. The X-axis shows KEGG pathways. b. Comparing with NKp44+ ILC3s, the numbers of downregulated (blue) and upregulated genes (red) are shown for NKp44− ILC3s. The Y-axis shows the

number of DEGs. The X-axis shows the KEGG pathways. c. Hierarchical clustering heatmaps of KEGG pathways depicting differential expression between NKp44+ and NKp44− ILC3s in the diseased and non-diseased regions from three patients with lung cancer. Gene expression changes (log2 fold-changes from their fragments per kilobase of transcript per million mapped reads values) are represented from lowest to highest as blue to red in the heat map; grey indicates that no gene transcript was detected.

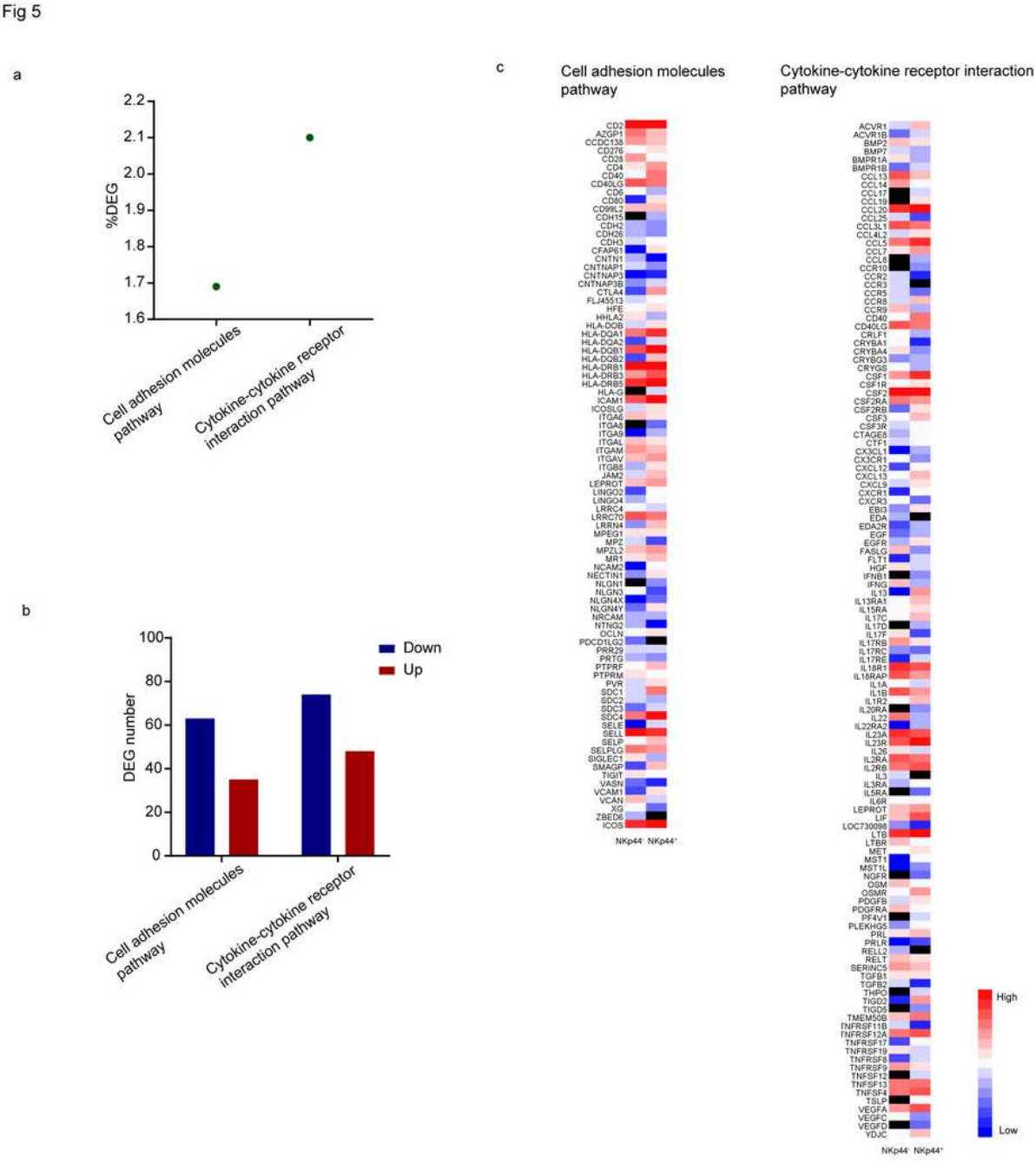

Figure 5

In the signaling molecules and interaction pathway, more differentially expressed genes (DEGs) were clustered in the cell adhesion molecules and cytokine-cytokine receptor interaction pathways. a. Percentages of DEGs in the cell adhesion molecules and cytokine-cytokine receptor interaction pathways. The Y-axis shows the percentages of DEGs out of total genes in the KEGG pathways. The X-axis shows the KEGG pathways. b. Comparing with NKp44+ group 3 innate lymphoid cells (ILC3s), the numbers of downregulated (blue) and upregulated genes (red) are shown for NKp44− ILC3s. The Y-axis shows the number of DEGs. The X-axis shows the KEGG pathways. c. Hierarchical clustering heatmaps of KEGG pathways depicting differential expression between NKp44+ and NKp44− ILC3s in the diseased and non-16 diseased regions from three patients with lung cancer. Gene expression changes (log2 fold-changes from their fragments per kilobase of transcript per million mapped reads values) are represented from lowest to highest as blue to red in the heat map; grey indicates that no gene transcript was detected.

Supplementary Files

This is a list of supplementary files associated with this preprint. Click to download.

- SupplementTalbe1.pdf
- SupplementTable2.pdf